Drift-Free and Self-Aligned IMU-Based Human Gait Tracking System With Augmented Precision and Robustness

Yawen Chen, Chenglong Fu, Winnie Suk Wai Leung, and Ling Shi

***Abstract*—IMU-based human joint motion acquisition system is attractive for real-time control and monitoring in the emerging wearable technology due to its portability. However, in practical applications, it heavily suffers from long-term drift, magnetic interference and inconsistency of rotational reference frames, which causes precision degradation. In this letter, a novel on-line IMU-based human gait estimation framework was proposed to obtain the joint rotational angles directly under the kinematic constraints between multiple body segments, whereas traditional methods need to estimate the orientation of each individual segment. This framework consists of an on-line algorithm to align IMU frames with human joints and motion estimation algorithms for hip and knee without the aid of magnetometer. Both a 2-DoF robot and human gait tests were performed to validate the proposed method as compared with the predictions from commercial IMUs, joint encoders and an optical tracking system. The outcome demonstrated its advantages of adaptive alignment, drift rejection and low computational cost, which alleviates the practical barriers faced by human motion data collection in the wearable devices.**

***Index Terms*—Human and humanoid motion analysis and synthesis, sensor fusion, adaptive alignment, drift rejection.**

I. Introduction

A. Human Motion Tracking Systems

HUMAN motion tracking systems have been widely utilized in medicine [1], biomechanics [2], humanoid robotics [3], film-making and games. There are several motion tracking methods such as marker-based optical tracking, image-based visual tracking [4], [5], exoskeleton-based mechanical tracking, and IMU-based (Inertial Measurement Unit) inertial tracking [6], [7]. The marker-based optical capture system contains multiple high-quality cameras to record the spatial positions of the markers attached at the human subject, which is precise but complex, expensive and unportable. The visual tracking method largely relies on image processing techniques and the results are usually not accurate enough [4], which can be improved with extra markers attached [5]. The mechanical tracking system uses a wearable exoskeleton with multiple degrees of freedom to move with the human subject, but it is difficult to align the mechanical rotational axis to the human joint, leading to measurement errors.

Among these tracking methods, IMU-based inertial tracking has attracted much attention due to its low cost and small size [8]. A tracking system typically consists of multiple IMUs to be attached at the body segments, which is easy to operate and portable. Moreover, it can achieve high sampling rate to be implemented for real-time control.

B. Orientation Estimation Algorithms of IMU

The orientation estimations from IMUs are usually not accurate enough with the effects of measurement noises and bias. The gyroscope obtains angular velocity of the module, by integrating of which the orientation can be estimated. The noises and bias, however, will introduce the integration drift. Therefore, the data from accelerometer and magnetometer providing the orientations relative to the gravitational and geomagnetic field are added to calibrate it.

Many algorithms have been designed to fuse the gyroscope data with the accelerometer and magnetometer data [8]. The Kalman filter is the most popular method based on the probabilistic models. Considering there exists a redundancy bias in the gyroscope data that can be modeled as a random walk, the indirect Kalman filter [9] or error-state Kalman filter [10] were designed by taking the orientation deviation as state. Besides, a gradient descent algorithm [11] was designed to optimize the orientation from gyroscope data by minimizing the estimation errors from accelerometer and magnetometer measurements, which achieved similar performance as the Kalman filter but with higher sampling rate.

C. Problems of IMU-Based Tracking Systems

Although IMU-based tracking system has attracted interests, in practical applications, it suffers from limitations such as long-term drift, magnetic interference and inconsistency.

In order to address long-term drift, generally, accelerometer and magnetometer data are involved [6], [7], [12].

Manuscript received February 14, 2020; accepted June 5, 2020. Date of publication June 15, 2020; date of current version June 29, 2020. This letter was recommended for publication by Associate Editor A. Escande and Editor A. Kheddar upon evaluation of the reviewers' comments. This work was supported by Shenzhen - Hong Kong Technology Cooperation Funding Scheme under Grants GHP-001-18SZ and SGLH20180619172011638. *(Corresponding author: Yawen Chen.)*

Yawen Chen and Ling Shi are with the Department of Electronic and Computer Engineering, The Hong Kong University of Science and Technology, Hong Kong 000000, China (e-mail: ychenga@connect.ust.hk; eesling@ust.hk).

Chenglong Fu is with the Department of Mechanical and Energy Engineering, Southern University of Science and Technology, Shenzhen 518055, China (e-mail: fucl@sustech.edu.cn).

Winnie Suk Wai Leung is with the Division of Integrative Systems and Design, The Hong Kong University of Science and Technology, Hong Kong 000000, China (e-mail: eewswleung@ust.hk).

This article has supplementary downloadable material available at https://ieeexplore.ieee.org, provided by the authors.

Digital Object Identifier 10.1109/LRA.2020.3002203

However, magnetometer data are easy to be disturbed [13], [14], resulting in tracking errors. Some commercial products used threshold-based approaches to reject the disturbance, which is effective only for sudden changes, hence limiting their practical uses.

To avoid using magnetometer data to eliminate drifts, in some researches, other sensors were involved to optimize the results, such as the cameras [15], [16], laser sensor [17] and UWB [18]. However, these methods have limited accuracy and increased the complexity of the tracking systems.

Moreover, the relative motion of the IMU attached at human body segment is regarded as the motion of that segment. In practice, the IMU coordinate frame is not aligned to the human joint, resulting in large tracking error. One popular solution is to calibrate the tracking system via specific body postures before using, such as N-pose and T-pose in Xsens MVN [6], [7] and upright posture [19], which are complex to operate and affected by the human states.

Considering the specific applications in human motion tracking, some researches tried to calibrate the tracking system subject to kinematic constraints. By assuming that the adjacent segments will rotate around fix joint axis or joint center [20], constraints on the rational direction of angular rate or/and acceleration of joint center are added to identify the transformation between IMU frames and human body frames, which has been implemented to track motions of elbow [21] and knee [22], [23]. However, magnetometer data are still involved in those researches, where magnetic disturbance will affect the calibration and tracking results. For acceleration constraints, the centripetal and coriolis accelerations are either ignored or estimated by prior known sensor positions [24], leading to estimation errors. Moreover, most researches are designed to estimate the joint axis off-line, after which motion tracking is conducted. Therefore, those methods still need calibration operations before tracking.

In this letter, a novel orientation estimation method for IMU-based tracking system is proposed to achieve easier operation, better precision and robustness. Considering the existing challenges of alignment calibration, drift and magnetic disturbance, following works have been performed.

1) An on-line self-calibration method was designed to find the alignment quaternions of IMUs related to the human segments. As a result, complex calibration before utilization can be avoided.
2) An approach to obtain orientations without drift was proposed using gyroscope and accelerometer data, by which geomagnetic disturbances do not affect.
3) An estimation algorithm with state representations in rotational angle was issued to obtain the human gait directly, thus avoiding process errors from quaternion normalization.
4) The estimation accuracy was investigated in comparison with commercial IMUs, joint encoders and an optical tracking system.

The proposed IMU-based tracking system is described and modeled in Section II. The gait estimation method and experiment results are detailed in Section III and IV, respectively. Finally, a conclusion is drawn in Section V.

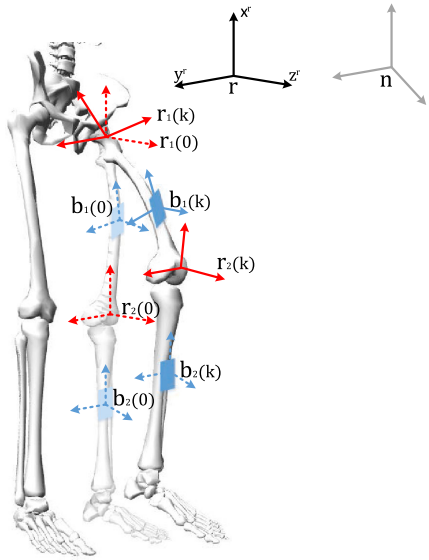

Fig. 1. An illustration of the coordinate frames in the IMU-based human gait tracking system.

II. Human Gait Tracking System and Modeling

A. System Descriptions

The IMU-based tracking system consists of four IMUs attached at the thighs and calves, respectively, to obtain the motion of hip and knee joints, shown as Fig. 1. In order to discuss the quantities of human motion and sensor measurements, the following coordinate frames are introduced.

- *The local navigation frame* $\mathbf{n}$ is the local geographic frame that is the east-north-up (ENU) frame.
- *The motion reference frame* $\mathbf{r}$ is attached at the human body and defined by the anatomy. The $\mathbf{x}$ and $\mathbf{y}$ axes are vertical to the transverse and sagittal plane, respectively, while $\mathbf{z}$ is vertical to the frontal plane and always points forward in the direction of walking.
- *The hip reference frame* $\mathbf{r}_1$ is attached at the hip joint and moves with the thigh. At neutral body posture, this frame is marked as $\mathbf{r}_1(0)$ and similar to frame $\mathbf{r}$. With the hip rotating, it is transformed to $\mathbf{r}_1(k)$ at time k.
- *The knee reference frame* $\mathbf{r}_2$ is attached at the knee joint and moves with the calf. Similar to the frame $\mathbf{r}_1$, it is marked as $\mathbf{r}_2(0)$ at the neutral body posture and transformed to $\mathbf{r}_2(k)$ with the knee rotating.
- *The body frame of the thigh* $\mathbf{b}_1$ and *The body frame of the calf* $\mathbf{b}_2$ are the coordinate frame of the IMU attached at thigh and calf.

Taking the human motion defined in anthropometry and anatomy into consideration, the basic assumptions about the above frames are stated below.

- At the neutral body posture, the frames of $\mathbf{r}_1(0)$ and $\mathbf{r}_2(0)$ coincide with the frame $\mathbf{r}$.
- The human subject will walk with small turning speed, then $\mathbf{r}$ is quasi-static and its motion can be ignored.
- The sagittal axes of hip and knee are always parallel to each other, meaning that $\mathbf{y}^{\mathbf{r}_2}(k)$ is parallel to $\mathbf{y}^{\mathbf{r}_1}(k)$ and knee joint only rotates around its sagittal axis $\mathbf{y}^{\mathbf{r}_2}(k)$.

- Since there is no reference for the rotation about the gravity axis, the hip joint is assumed to move with only flexion-extension and adduction-abduction, and the rotation about $\mathbf{x}^{\mathbf{r}_1}(k)$ is ignored.

Therefore, the human gait can be defined based on the above assumptions and coordinate frames. The motion of knee θ_2 is described by the rotational angle about $\mathbf{y}^{\mathbf{r}_2}(k)$ between the frames of $\mathbf{r}_1(k)$ and $\mathbf{r}_2(k)$. The flexion of hip θ_1 is the rotational angle along $\mathbf{y}^{\mathbf{r}_1}(k)$ between the frames of $\mathbf{r}$ and $\mathbf{r}_1(k)$, while the adduction ϕ_1 is the angle between $\mathbf{y}^{r_1}(k)$ and transverse plane.

In the following sections, $\mathbf{R}_{\mathbf{a}}^{\mathbf{b}} \in \mathbb{R}^{3\times3}$ and $\mathbf{q}_{\mathbf{a}}^{\mathbf{b}} \in \mathbb{R}^4$ represent the rotational matrix and quaternion of frame $\mathbf{b}$ relative to frame $\mathbf{a}$, while ${}^{\mathbf{a}}\mathbf{v} \in \mathbb{R}^3$ is the vector expressed in frame $\mathbf{a}$.

B. System Modeling

In order to estimate the rotational angles of hip and knee joints, we firstly delineate the transform relationships between the coordinate frames in this tracking system. At the initial neutral body posture, we have

$$\mathbf{q}_{\mathbf{r}}^{\mathbf{r}_1}(0) = \mathbf{q}_{\mathbf{r}}^{\mathbf{r}_2}(0) = \mathbf{q}_{\mathbf{r}_1}^{\mathbf{r}_2}(0) = [1,0,0,0]^T \tag{1}$$

$$\phi_1(0) = \theta_1(0) = \theta_2(0) = 0 \tag{2}$$

With the human subject walking, at time k, the gait motion is described by the flexion $\theta_1(k)$ and adduction $\phi_1(k)$ of hip, as well as the flexion $\theta_2(k)$ of knee. The relations between joint angles and rotational quaternions can be obtained by the definition and assumptions from Section II. The operator $\otimes$ represents quaternion multiplication.

$$\mathbf{q}_{\mathbf{r}}^{\mathbf{r}_1}(k) = \mathbf{q}\left(y, \theta_1(k)\right) \otimes \mathbf{q}\left(z, \phi_1(k)\right) \tag{3}$$

$$\mathbf{q}_{\mathbf{r}_1}^{\mathbf{r}_2}(k) = \mathbf{q}\left(y, \theta_2(k)\right) \tag{4}$$

$$\mathbf{q}\left(z, \phi_i\right) = \left[\cos\left(\frac{\phi_i}{2}\right); \mathbf{c}_{\mathbf{z}} \sin\left(\frac{\phi_i}{2}\right)\right] \tag{5}$$

$$\mathbf{q}\left(y, \theta_i\right) = \left[\cos\left(\frac{\theta_i}{2}\right); \mathbf{c}_{\mathbf{y}} \sin\left(\frac{\theta_i}{2}\right)\right] \tag{6}$$

where $\mathbf{c}_{\mathbf{y}} = [0,1,0]^T$, $\mathbf{c}_{\mathbf{z}} = [0,0,1]^T$, $i = 1$ or 2.

From the general orientation estimation algorithms for IMU, the relation between angular velocity and rotational quaternion is designed as the system dynamics for priori estimation, after which the estimation is optimized by the gravity measurement. Let ${}^{\mathbf{r}_1}\mathbf{w}_{\mathbf{r}}^{\mathbf{r}_1}(k)$ and ${}^{\mathbf{r}_2}\mathbf{w}_{\mathbf{r}}^{\mathbf{r}_2}(k)$ be the angular velocities of frames $\mathbf{r}_1(k)$ and $\mathbf{r}_2(k)$ at time k, the quaternion derivatives can be calculated by kinematics.

$$\frac{\mathrm{d}\mathbf{q}_{\mathbf{r}}^{\mathbf{r}_1}(k)}{\mathrm{d}t} = \frac{1}{2}\begin{bmatrix} 0 \\ {}^{\mathbf{r}_1}\mathbf{w}_{\mathbf{r}}^{\mathbf{r}_1}(k) \end{bmatrix} \otimes \mathbf{q}_{\mathbf{r}}^{\mathbf{r}_1}(k) \tag{7}$$

$$\frac{\mathrm{d}\mathbf{q}_{\mathbf{r}_1}^{\mathbf{r}_2}(k)}{\mathrm{d}t} = \frac{1}{2}\begin{bmatrix} 0 \\ {}^{\mathbf{r}_2}\mathbf{w}_{\mathbf{r}_1}^{\mathbf{r}_2}(k) \end{bmatrix} \otimes \mathbf{q}_{\mathbf{r}_1}^{\mathbf{r}_2}(k) \tag{8}$$

$${}^{\mathbf{r}_2}\mathbf{w}_{\mathbf{r}_1}^{\mathbf{r}_2}(k) = {}^{\mathbf{r}_2}\mathbf{w}_{\mathbf{r}}^{\mathbf{r}_2}(k) - \mathbf{R}\left(\mathbf{q}_{\mathbf{r}_1}^{\mathbf{r}_2}(k)\right) {}^{\mathbf{r}_1}\mathbf{w}_{\mathbf{r}}^{\mathbf{r}_1}(k) \tag{9}$$

Let ${}^{\mathbf{r}_1}\mathbf{g}(k)$ and ${}^{\mathbf{r}_2}\mathbf{g}(k)$ be the gravity vectors expressed in the frames $\mathbf{r}_1(k)$ and $\mathbf{r}_2(k)$ at time k, they can be calculated by rotational transformation with ${}^{\mathbf{r}}\mathbf{g} = [1,0,0]^T$, the gravity vector expressed in the frame $\mathbf{r}$.

$${}^{\mathbf{r}_1}\mathbf{g}(k) = \mathbf{R}\left(\mathbf{q}_{\mathbf{r}}^{\mathbf{r}_1}(k)\right) {}^{\mathbf{r}}\mathbf{g} \tag{10}$$

$${}^{\mathbf{r}_2}\mathbf{g}(k) = \mathbf{R}\left(\mathbf{q}_{\mathbf{r}_1}^{\mathbf{r}_2}(k)\right) \mathbf{R}\left(\mathbf{q}_{\mathbf{r}}^{\mathbf{r}_1}(k)\right) {}^{\mathbf{r}}\mathbf{g} \tag{11}$$

For each IMU in the system, the tri-axis gyroscope obtains three dimensional angular rate ${}^{b}\mathbf{w}_{n}^{b}$ in body frame, where the measurement $\mathbf{y}_w$ is affected by gyroscope bias $\mathbf{b}_w$ and noise $\mathbf{n}_w$. The bias is modeled as random walk with derivative in Gaussian distribution $\dot{\mathbf{b}}_w = \mathbf{n}_{bw} \sim N(0, \Sigma_{b_w})$, while the gyroscope noise as Gaussian white noise $\mathbf{n}_w \sim N(0, \Sigma_w)$. The tri-axis accelerometer measures the three dimensional external force of the sensor. Ignoring the motion acceleration that is small during human walking, the accelerometer measurement $\mathbf{y}_a$ contains the gravity $\mathbf{g}$ in body frame and Gaussian white noise $\mathbf{n}_a \sim N(0, \Sigma_a)$.

$$\mathbf{y}_w = {}^{b}\mathbf{w}_{n}^{b} + \mathbf{b}_w + \mathbf{n}_w \tag{12}$$

$$\mathbf{y}_a = -\mathbf{R}(\mathbf{q}_{n}^{b})\, {}^{n}\mathbf{g} + \mathbf{n}_a \tag{13}$$

After the IMUs are attached, the body frames of them are aligned to the joint reference frames by $\mathbf{q}_{\mathbf{b}_1}^{\mathbf{r}_1}$ and $\mathbf{q}_{\mathbf{b}_2}^{\mathbf{r}_2}$, which are unknown and need to be estimated. Let ${}^{\mathbf{b}_i}\hat{\mathbf{w}}_{\mathbf{n}}^{\mathbf{b}_i}(k)$ and ${}^{\mathbf{b}_i}\hat{\mathbf{g}}(k)$ be the estimations of angular rate and gravity for $\mathbf{b}_i$. Due to the assumption that $\mathbf{r}$ is quasi-static, the angular velocities of joint frames $\mathbf{r}_i$ relative to $\mathbf{r}$ and gravity force can be obtained as follows.

$${}^{\mathbf{r}_i}\hat{\mathbf{w}}_{\mathbf{r}}^{\mathbf{r}_i}(k) = \mathbf{R}\left(\mathbf{q}_{\mathbf{b}_i}^{\mathbf{r}_i}\right) {}^{\mathbf{b}_i}\hat{\mathbf{w}}_{\mathbf{n}}^{\mathbf{b}_i}(k) \tag{14}$$

$${}^{\mathbf{r}_i}\hat{\mathbf{g}}(k) = \mathbf{R}\left(\mathbf{q}_{\mathbf{b}_i}^{\mathbf{r}_1}\right) {}^{\mathbf{b}_i}\hat{\mathbf{g}}(k) \tag{15}$$

C. Problem Statements

In the real-time tracking system, the IMUs measurement data of $\{\mathbf{y}_w^{\mathbf{b}_1}(k), \mathbf{y}_w^{\mathbf{b}_2}(k), \mathbf{y}_g^{\mathbf{b}_1}(k), \mathbf{y}_g^{\mathbf{b}_2}(k)\}$ are acquired as the estimations of $\{{}^{\mathbf{b}_1}\hat{\mathbf{w}}_{\mathbf{n}}^{\mathbf{b}_1}(k), {}^{\mathbf{b}_2}\hat{\mathbf{w}}_{\mathbf{n}}^{\mathbf{b}_2}(k), {}^{\mathbf{b}_1}\hat{\mathbf{g}}(k), {}^{\mathbf{b}_2}\hat{\mathbf{g}}(k)\}$ referred to (12) and (13). As there are biases and noises in the measurements, we use the angular velocity and rotational dynamics to estimate the quaternion firstly, and then improve the estimation by minimizing the error in gravity measurement. To avoid orientation drift without geomagnetic data, the constraints for human motion are involved. Therefore,

Problem 1: Hip joint angle estimation

$$\begin{aligned} \min_{\hat{\phi}_1(k), \hat{\theta}_1(k), \hat{\mathbf{q}}_{\mathbf{b}_1}^{\mathbf{r}_1}} \quad & f_1 = \left|\left|\mathbf{R}\left(\hat{\mathbf{q}}_{\mathbf{r}}^{\mathbf{r}_1}(k)\right) {}^{\mathbf{r}}\mathbf{g} - \mathbf{R}\left(\hat{\mathbf{q}}_{\mathbf{b}_1}^{\mathbf{r}_1}\right) \mathbf{y}_g^{\mathbf{b}_1}(k)\right|\right|_2^2 \\ \text{subject to} \quad & {}^{\mathbf{r}_1}\hat{\mathbf{w}}_{\mathbf{r}}^{\mathbf{r}_1}(k) = \mathbf{R}\left(\hat{\mathbf{q}}_{\mathbf{b}_1}^{\mathbf{r}_1}\right) \mathbf{y}_w^{\mathbf{b}_1}(k) \\ & \frac{\mathrm{d}\hat{\mathbf{q}}_{\mathbf{r}}^{\mathbf{r}_1}(k)}{dt} = \frac{1}{2}\begin{bmatrix} 0 \\ {}^{\mathbf{r}_1}\hat{\mathbf{w}}_{\mathbf{r}}^{\mathbf{r}_1}(k) \end{bmatrix} \otimes \hat{\mathbf{q}}_{\mathbf{r}}^{\mathbf{r}_1}(k-1) \\ & \hat{\mathbf{q}}_{\mathbf{r}}^{\mathbf{r}_1}(k) = \mathbf{q}\left(y, \hat{\theta}_1(k)\right) \otimes \mathbf{q}\left(z, \hat{\phi}_1(k)\right) \end{aligned} \tag{16}$$

Problem 2: Knee joint angle estimation

$$\begin{aligned} \min_{\hat{\theta}_2(k), \hat{\mathbf{q}}_{\mathbf{b}_1}^{\mathbf{r}_1}, \hat{\mathbf{q}}_{\mathbf{b}_2}^{\mathbf{r}_2}} \quad & f_2 = \left|\left|\mathbf{R}\left(\hat{\mathbf{q}}_{\mathbf{r}_1}^{\mathbf{r}_2}(k) \otimes \hat{\mathbf{q}}_{\mathbf{b}_1}^{\mathbf{r}_1}\right) \mathbf{y}_g^{\mathbf{b}_1}(k)\right.\right. \\ & \qquad \left.\left. - \mathbf{R}\left(\hat{\mathbf{q}}_{\mathbf{b}_2}^{\mathbf{r}_2}\right) \mathbf{y}_g^{\mathbf{b}_2}(k)\right|\right|_2^2 \\ \text{subject to} \quad & {}^{\mathbf{r}_2}\hat{\mathbf{w}}_{\mathbf{r}_1}^{\mathbf{r}_2}(k) = \mathbf{R}\left(\hat{\mathbf{q}}_{\mathbf{b}_2}^{\mathbf{r}_2}\right) \mathbf{y}_w^{\mathbf{b}_2}(k) \\ & \qquad - \mathbf{R}\left(\hat{\mathbf{q}}_{\mathbf{r}_1}^{\mathbf{r}_2} \otimes \hat{\mathbf{q}}_{\mathbf{b}_1} eq^{\mathbf{r}_1}\right) \mathbf{y}_w^{\mathbf{b}_1}(k) \\ & \frac{\mathrm{d}\hat{\mathbf{q}}_{\mathbf{r}_1}^{\mathbf{r}_2}(k)}{\mathrm{d}t} = \frac{1}{2}\begin{bmatrix} 0 \\ {}^{\mathbf{r}_2}\hat{\mathbf{w}}_{\mathbf{r}_1}^{\mathbf{r}_2}(k) \end{bmatrix} \otimes \hat{\mathbf{q}}_{\mathbf{r}_1}^{\mathbf{r}_2}(k-1) \end{aligned}$$

$$\hat{\mathbf{q}}_{\mathbf{r}_1}^{\mathbf{r}_2}(k) = \mathbf{q}\left(y, \hat{\theta}_2(k)\right) \tag{17}$$

In the above optimizations, the objective functions use the acceleration measurements to correct the integral drifts from gyroscope data, where the motion accelerations are typically ignored as they are comparably small during human walking. The first two constraints describe the angular rates and quaternion dynamics, while the last one represents human kinematic constraint from system assumptions.

However, it is extremely difficult to solve them, as all the variables to be estimated are influenced by each other. The alignment quaternions $\hat{\mathbf{q}}_{\mathbf{b}_1}^{\mathbf{r}_1}$ and $\hat{\mathbf{q}}_{\mathbf{b}_2}^{\mathbf{r}_2}$ are unknown and will affect the calculation of ${}^{\mathbf{r}_1}\hat{\mathbf{w}}_{\mathbf{r}}^{\mathbf{r}_1}(k)$ and ${}^{\mathbf{r}_2}\hat{\mathbf{w}}_{\mathbf{r}_1}^{\mathbf{r}_2}(k)$, while the angular velocities will determine the rotational quaternions and then the cost functions.

III. Human Gait Estimation Method

A. Relaxation of the Human Gait Tracking Problem

The IMU-based tracking system with human kinematic constraints is analyzed to introduce the two problems for hip and knee joint angle estimation. In order to solve the interdependence of alignment quaternions and joint rotational angles, in this letter, the original problems are divided into three subproblems, which are then optimized in each sample.

Problem 3: Equivalent subproblems to solve P1 and P2

1) The estimation of alignment quaternions $\hat{\mathbf{q}}_{\mathbf{b}_1}^{\mathbf{r}_1}$ and $\hat{\mathbf{q}}_{\mathbf{b}_2}^{\mathbf{r}_2}$, with the kinematic constraint that knee joint only rotates around its sagittal axis.
2) The estimation of knee joint angle $\theta_2(k)$, based on (17) and the latest $\hat{\mathbf{q}}_{\mathbf{b}_1}^{\mathbf{r}_1}$ and $\hat{\mathbf{q}}_{\mathbf{b}_2}^{\mathbf{r}_2}$.
3) The estimation of hip joint angles $\phi_1(k)$ and $\theta_1(k)$, based on (16) and the latest $\hat{\mathbf{q}}_{\mathbf{b}_1}^{\mathbf{r}_1}$.

B. The Estimation of Alignment Quaternions

These two alignment rotational quaternions determine the angular velocity estimations of the joints, which must satisfy the human walking features. From the assumption that knee joint only rotates around $\mathbf{y}^{\mathbf{r}_2(k)}$, the constraint about ${}^{\mathbf{r}_2}\hat{\mathbf{w}}_{\mathbf{r}_1}^{\mathbf{r}_2}(k)$ is designed to optimize the $\hat{\mathbf{q}}_{\mathbf{b}_1}^{\mathbf{r}_1}$ and $\hat{\mathbf{q}}_{\mathbf{b}_2}^{\mathbf{r}_2}$ estimations.

$$\mathbf{c}_{\mathbf{y}} \times {}^{\mathbf{r}_2}\mathbf{w}_{\mathbf{r}_1}^{\mathbf{r}_2}(k) = \mathbf{0} \tag{18}$$

However, both $\hat{\mathbf{q}}_{\mathbf{b}_1}^{\mathbf{r}_1}$ and $\hat{\mathbf{q}}_{\mathbf{b}_2}^{\mathbf{r}_2}$ have three independent variables, equation (18) is not enough to solve them. One method is to consider the velocity series for a long duration, which is similar to the off-line calibration process in [20]. For on-line alignment, other conditions are needed.

After the IMUs are worn by the human subject, at the static neutral body posture, the orientation of each IMU except heading can be estimated by the measured gravity. That orientation can be treated as part of the alignment transformation, as the hip reference frame $\mathbf{r}_1$ and hip reference frame $\mathbf{r}_2$ are defined to coincide with $\mathbf{r}$ at the initial posture. Then, the $\hat{\mathbf{q}}_{\mathbf{b}_1}^{\mathbf{r}_1}$ and $\hat{\mathbf{q}}_{\mathbf{b}_2}^{\mathbf{r}_2}$ are divided into two parts. One is the rotational quaternion $\hat{\mathbf{q}}_{\mathbf{b}_i}$ estimated at the beginning, while the other is the heading angle $\hat{\psi}_i$ optimized by knee motion constraint.

$$\hat{\mathbf{q}}_{\mathbf{b}_i}^{\mathbf{r}_i} = \mathbf{q}\left(x, \hat{\psi}_i\right) \otimes \hat{\mathbf{q}}_{\mathbf{b}_i} \tag{19}$$

$$\hat{\mathbf{q}}_{\mathbf{b}_i} = \arg\min ||\hat{\mathbf{q}}_{\mathbf{b}_i}{}^{\mathbf{r}}\mathbf{g} - \mathbf{y}_g^{\mathbf{b}_i}(0)||_2^2 \tag{20}$$

Therefore, the estimation of $\hat{\mathbf{q}}_{\mathbf{b}_1}^{\mathbf{r}_1}$ and $\hat{\mathbf{q}}_{\mathbf{b}_2}^{\mathbf{r}_2}$ becomes the problem to optimize $\hat{\psi}_1$ and $\hat{\psi}_2$.

Problem 3.1: Estimation of alignment quaternions

$$\min_{\hat{\psi}_1, \hat{\psi}_2} \quad h_{\text{align}} = ||\mathbf{c}_{\mathbf{y}} \times {}^{\mathbf{r}_2}\mathbf{w}_{\mathbf{r}_1}^{\mathbf{r}_2}(k)||_2^2 \tag{21}$$

Referred to ${}^{\mathbf{r}_2}\mathbf{w}_{\mathbf{r}_1}^{\mathbf{r}_2}(k)$ in (17) and $\hat{\mathbf{q}}_{\mathbf{b}_i}^{\mathbf{r}_i}$ in (19).

$$\begin{aligned} h_{\text{align}} &= ||[\mathbf{c}_{\mathbf{y}}\times]\mathbf{R}\left(\mathbf{q}\left(x, \hat{\psi}_2\right)\right)\mathbf{R}\left(\hat{\mathbf{q}}_{\mathbf{b}_2}\right)\mathbf{y}_w^{\mathbf{b}_2}(k) \\ &\quad - [\mathbf{c}_{\mathbf{y}}\times]\mathbf{R}\left(\mathbf{q}\left(x, \hat{\psi}_1\right)\right)\mathbf{R}\left(\hat{\mathbf{q}}_{\mathbf{b}_1}\right)\mathbf{y}_w^{\mathbf{b}_1}(k)||_2^2 \\ &= ||[\tilde{\mathbf{y}}_w^{\mathbf{b}_2}(k)\times]\mathbf{v}(\hat{\psi}_2) - [\tilde{\mathbf{y}}_w^{\mathbf{b}_1}(k)\times]\mathbf{v}(\hat{\psi}_1)||_2^2 \end{aligned} \tag{22}$$

$$\tilde{\mathbf{y}}_w^{\mathbf{b}_i}(k) = \mathbf{R}\left(\hat{\mathbf{q}}_{\mathbf{b}_i}\right)\mathbf{y}_w^{\mathbf{b}_i}(k) \tag{23}$$

$$\mathbf{v}(\hat{\psi}_i) = [0, \cos(\hat{\psi}_i), \sin(\hat{\psi}_i)]^T \tag{24}$$

Through gradient descent method,

$$\begin{aligned} \frac{\partial h_{\text{align}}}{\partial \mathbf{v}(\hat{\psi}_i)} &= 2\mathbf{v}^T(\hat{\psi}_i)[\tilde{\mathbf{y}}_w^{\mathbf{b}_i}(k)\times]^T[\tilde{\mathbf{y}}_w^{\mathbf{b}_i}(k)\times] \\ &\quad - 2\mathbf{v}^T(\hat{\psi}_j)[\tilde{\mathbf{y}}_w^{\mathbf{b}_j}\times]^T[\tilde{\mathbf{y}}_w^{\mathbf{b}_i}(k)\times] \end{aligned} \tag{25}$$

$$\frac{\mathrm{d}\mathbf{v}(\hat{\psi}_i)}{\mathrm{d}(\hat{\psi}_i)} = [0, -\sin(\hat{\psi}_i), \cos(\hat{\psi}_i)]^T \tag{26}$$

$$\hat{\psi}_i(k) = \hat{\psi}_i(k-1) - \alpha_i \frac{\partial h_{\text{align}}}{\partial \mathbf{v}(\hat{\psi}_i)} \frac{\mathrm{d}\mathbf{v}(\hat{\psi}_i)}{\mathrm{d}(\hat{\psi}_i)} \tag{27}$$

where $j = 2$ with $i = 1$, and $j = 1$ with $i = 2$, representing the position of IMU to be aligned. α_i is the parameter for the gradient descent algorithm, which can be a constant or obtained by line search. With large step size α_i, the alignment quaternions will converge quickly but may experience oscillations around the optimal point, while small α_i will result in slow convergence. By adjusting α_i, it generally takes one or two walking steps for the alignment quaternions to converge, before which inaccurate results will influence the estimation of angular velocity. At these sampling periods, the gravity vector should take more weights (that is high β_i) in the next joint angle estimation algorithms.

C. The Estimation of Knee Joint Angle

After alignment quaternions obtained, the knee motion can then be estimated by solving the optimization problem of (17) with the known $\hat{\mathbf{q}}_{\mathbf{b}_1}^{\mathbf{r}_1}$ and $\hat{\mathbf{q}}_{\mathbf{b}_2}^{\mathbf{r}_2}$. Due to the kinematic constraints, it is complex to solve the problem in quaternion, which is transformed in terms of rotational angle $\hat{\theta}_2(k)$.

Problem 3.2: Estimation of knee joint angle

$$\begin{aligned} \min_{\hat{\theta}_2(k)} \quad & f_2 = ||\mathbf{R}\left(y, \hat{\theta}_2(k)\right)\hat{\mathbf{y}}_g^{\mathbf{r}_1}(k) - \hat{\mathbf{y}}_g^{\mathbf{r}_2}(k)||_2^2 \\ \text{subject to} \quad & {}^{\mathbf{r}_2}\hat{\mathbf{w}}_{\mathbf{r}_1}^{\mathbf{r}_2}(k) = \hat{\mathbf{y}}_w^{\mathbf{r}_2}(k) - \mathbf{R}\left(\hat{\mathbf{q}}_{\mathbf{r}_1}^{\mathbf{r}_2}\right)\hat{\mathbf{y}}_w^{\mathbf{r}_1}(k) \\ & \mathrm{d}\hat{\theta}_2(k)/\mathrm{d}t = \mathbf{c}_{\mathbf{y}}^T \cdot {}^{\mathbf{r}_2}\hat{\mathbf{w}}_{\mathbf{r}_1}^{\mathbf{r}_2}(k) \\ & \hat{\mathbf{y}}_g^{\mathbf{r}_i}(k) = \mathbf{R}\left(\hat{\mathbf{q}}_{\mathbf{b}_i}^{\mathbf{r}_i}\right)\mathbf{y}_g^{\mathbf{b}_i}(k) \\ & \hat{\mathbf{y}}_w^{\mathbf{r}_i}(k) = \mathbf{R}\left(\hat{\mathbf{q}}_{\mathbf{b}_i}^{\mathbf{r}_i}\right)\mathbf{y}_w^{\mathbf{b}_i}(k) \end{aligned} \tag{28}$$

Algorithm 1: Estimation of $\hat{\mathbf{q}}_{\mathbf{b}_1}^{\mathbf{r}_1}$ and $\hat{\mathbf{q}}_{\mathbf{b}_2}^{\mathbf{r}_2}$.

Input
Initial alignment quaternion: $\hat{\mathbf{q}}_{\mathbf{b}_1}$, $\hat{\mathbf{q}}_{\mathbf{b}_2}$
Angular rates from IMUs: $\mathbf{y}_w^{\mathbf{b}_1}(k), \mathbf{y}_w^{\mathbf{b}_2}(k)$
Last estimations: $\hat{\psi}_1(k-1), \hat{\psi}_2(k-1)$
Output
Latest estimations: $\hat{\psi}_1(k), \hat{\psi}_2(k)$
Latest alignment quaternion: $\hat{\mathbf{q}}_{\mathbf{b}_1}^{\mathbf{r}_1}(k), \hat{\mathbf{q}}_{\mathbf{b}_2}^{\mathbf{r}_2}(k)$
Convergence flag: β_f

Calculate $\tilde{\mathbf{y}}_w^{\mathbf{b}_1}(k)$, $\tilde{\mathbf{y}}_w^{\mathbf{b}_2}(k)$, $\mathbf{v}(\hat{\psi}_1)$, $\mathbf{v}(\hat{\psi}_2)$ by (23), (24)
Calculate $\frac{\partial h_{\text{align}}}{\partial \mathbf{v}(\hat{\psi}_i)}$ and $\frac{\mathrm{d}\mathbf{v}(\hat{\psi}_i)}{\mathrm{d}(\hat{\psi}_i)}$ by (22), (25), (26)
Then $\hat{\psi}_i(k) = \hat{\psi}_i(k-1) - \alpha_i \frac{\partial h_{\text{align}}}{\partial \mathbf{v}(\hat{\psi}_i)} \frac{\mathrm{d}\mathbf{v}(\hat{\psi}_i)}{\mathrm{d}(\hat{\psi}_i)}$
$\hat{\mathbf{q}}_{\mathbf{b}_i}^{\mathbf{r}_i} = \mathbf{q}(x, \hat{\psi}_i(k)) \otimes \hat{\mathbf{q}}_{\mathbf{b}_i}$
if $|\hat{\psi}_i(k) - \hat{\psi}_i(k-1)|$ Converge**then**
$\beta_f = 1$
end if

Adapted from [11], the data fusion algorithm is designed by combining the estimated gradients from angular velocity and gravity vector. From the objective function with gravity,

$$\frac{\mathrm{d}f_2}{\mathrm{d}\hat{\theta}_2} = -2\left(\hat{\mathbf{y}}_g^{\mathbf{r}_2}(k)\right)^T \frac{\mathrm{d}\mathbf{R}\left(y, \hat{\theta}_2(k)\right)}{\mathrm{d}\hat{\theta}_2} \hat{\mathbf{y}}_g^{\mathbf{r}_1}(k) \tag{29}$$

$$\frac{\mathrm{d}\mathbf{R}}{\mathrm{d}\hat{\theta}_2} = \begin{bmatrix} -\sin(\hat{\theta}_2) & 0 & -\cos(\hat{\theta}_2) \\ 0 & 0 & 0 \\ \cos(\hat{\theta}_2) & 0 & -\sin(\hat{\theta}_2) \end{bmatrix} \tag{30}$$

Then the rotational angle is obtained by complementary filter.

$$\Delta\hat{\theta}_2(k) = \mathbf{c}_{\mathbf{y}}^T \cdot {}^{\mathbf{r}_2}\hat{\mathbf{w}}_{\mathbf{r}_1}^{\mathbf{r}_2}(k)\Delta t - \beta_2 \frac{\mathrm{d}f_2}{\mathrm{d}\hat{\theta}_2} \tag{31}$$

$$\hat{\theta}_2(k) = \hat{\theta}_2(k-1) + \Delta\hat{\theta}_2(k) \tag{32}$$

where β_2 represents the estimation error magnitude of angular rate from gyroscope related to accelerometer measurement, which can be regulated to adjust the confidence of angular velocity and gravity vector. Before the convergence of alignment quaternions, the angular rate estimations are not very accurate due to the incorrect alignment quaternions. Therefore, a high β_2 should be chosen with higher weight on acceleration. Once the alignment quaternions converge, a low β_2 can be taken with more confidence on angular rate.

D. The Estimation of Hip Joint Angle

Similar to the estimation algorithm for knee joint, the optimization problem for hip joint motion is transformed with the states of $\hat{\phi}_1(k)$ and $\hat{\theta}_1(k)$, while the gradient of cost function is computed in two degrees of freedom.

Problem 3.3: Estimation of hip joint angle

$$\min_{\hat{\phi}_1(k), \hat{\theta}_1(k)} \quad f_1 = \left|\left|\mathbf{R}\left(y, \hat{\theta}_1(k)\right)\mathbf{R}\left(z, \hat{\phi}_1(k)\right){}^{\mathbf{r}}\mathbf{g} - \hat{\mathbf{y}}_g^{\mathbf{r}_1}(k)\right|\right|_2^2$$

$$\text{subject to} \quad {}^{\mathbf{r}_1}\hat{\mathbf{w}}_{\mathbf{r}}^{\mathbf{r}_1}(k) = \hat{\mathbf{y}}_w^{\mathbf{r}_1}(k) = \mathbf{R}\left(\hat{\mathbf{q}}_{\mathbf{b}_1}^{\mathbf{r}_1}\right)\mathbf{y}_w^{\mathbf{b}_1}(k)$$

$$\mathrm{d}\hat{\phi}_1(k)/\mathrm{d}t = \mathbf{c}_{\mathbf{z}}^T \cdot {}^{\mathbf{r}_1}\hat{\mathbf{w}}_{\mathbf{r}}^{\mathbf{r}_1}(k)$$

Algorithm 2: Estimation of $\hat{\theta}_2(k)$.

Input
Latest alignment quaternion: $\hat{\mathbf{q}}_{\mathbf{b}_1}^{\mathbf{r}_1}(k)$, $\hat{\mathbf{q}}_{\mathbf{b}_2}^{\mathbf{r}_2}(k)$
Angular rates from IMUs: $\mathbf{y}_w^{\mathbf{b}_1}(k), \mathbf{y}_w^{\mathbf{b}_2}(k)$
Acceleration from IMUs: $\mathbf{y}_g^{\mathbf{b}_1}(k), \mathbf{y}_g^{\mathbf{b}_2}(k)$
Last estimations: $\hat{\theta}_2(k-1)$
Alignment quaternion convergence flag: β_f
Output
Knee joint angle: $\hat{\theta}_2(k)$

Calculate $\hat{\mathbf{y}}_w^{\mathbf{r}_1}(k)$, $\hat{\mathbf{y}}_w^{\mathbf{r}_2}(k)$, $\hat{\mathbf{y}}_g^{\mathbf{r}_1}(k)$, $\hat{\mathbf{y}}_g^{\mathbf{r}_2}(k)$ and ${}^{\mathbf{r}_2}\hat{\mathbf{w}}_{\mathbf{r}_1}^{\mathbf{r}_2}(k)$
Calculate $\frac{\mathrm{d}f_2}{\mathrm{d}\hat{\theta}_2}$ by (29)
if $\beta_f == 1$ Alignment quaternions converge **then**
  $\beta_2 = \beta_2(low)$
else
  $\beta_2 = \beta_2(high)$
end if
$\Delta\hat{\theta}_2(k) = \mathbf{c}_{\mathbf{y}}^T \cdot {}^{\mathbf{r}_2}\hat{\mathbf{w}}_{\mathbf{r}_1}^{\mathbf{r}_2}(k)\Delta t - \beta_2 \frac{\mathrm{d}f_2}{\mathrm{d}\hat{\theta}_2}$
$\hat{\theta}_2(k) = \hat{\theta}_2(k-1) + \Delta\hat{\theta}_2(k)$
$\hat{\mathbf{q}}_{\mathbf{r}_1}^{\mathbf{r}_2}(k) = \mathbf{q}(y, \hat{\theta}_2(k))$

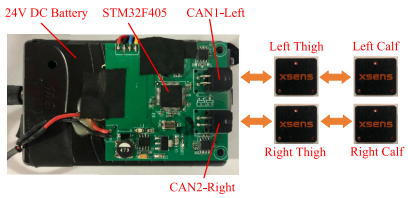

Fig. 2. The experimental hardware of IMU-based tracking system.

$$\mathrm{d}\hat{\theta}_1(k)/\mathrm{d}t = \mathbf{c}_{\mathbf{y}}^T \cdot {}^{\mathbf{r}_1}\hat{\mathbf{w}}_{\mathbf{r}}^{\mathbf{r}_1}(k)$$

$$\hat{\mathbf{y}}_g^{\mathbf{b}_1}(k) = \mathbf{R}\left(\hat{\mathbf{q}}_{\mathbf{b}_1}^{\mathbf{r}_1}\right)\mathbf{y}_g^{\mathbf{b}_1}(k) \tag{33}$$

For the problem with two variables to be optimized, it is solved as follows.

$$\frac{\mathrm{d}f_1}{\mathrm{d}\hat{\phi}_1} = -2\left(\hat{\mathbf{y}}_g^{\mathbf{r}_1}(k)\right)^T \mathbf{R}\left(y, \hat{\theta}_1(k)\right) \frac{\mathrm{d}\mathbf{R}\left(z, \hat{\phi}_1(k)\right)}{\mathrm{d}\hat{\phi}_1} {}^{\mathbf{r}}\mathbf{g} \tag{34}$$

$$\frac{\mathrm{d}f_1}{\mathrm{d}\hat{\theta}_1} = -2\left(\hat{\mathbf{y}}_g^{\mathbf{r}_1}(k)\right)^T \frac{\mathrm{d}\mathbf{R}\left(y, \hat{\theta}_1(k)\right)}{\mathrm{d}\hat{\theta}_1} \mathbf{R}\left(z, \hat{\phi}_1(k)\right) {}^{\mathbf{r}}\mathbf{g} \tag{35}$$

$$\frac{\mathrm{d}\mathbf{R}}{\mathrm{d}\hat{\phi}_1} = \begin{bmatrix} -\sin(\hat{\phi}_1) & \cos(\hat{\phi}_1) & 0 \\ -\cos(\hat{\phi}_1) & -\sin(\hat{\phi}_1) & 0 \\ 0 & 0 & 0 \end{bmatrix} \tag{36}$$

$$\frac{\mathrm{d}\mathbf{R}}{\mathrm{d}\hat{\theta}_1} = \begin{bmatrix} -\sin(\hat{\theta}_1) & 0 & -\cos(\hat{\theta}_1) \\ 0 & 0 & 0 \\ \cos(\hat{\theta}_1) & 0 & -\sin(\hat{\theta}_1) \end{bmatrix} \tag{37}$$

IV. Experiment Results

A. Implementation Details

An experimental version of the IMU-based tracking system was designed, shown in Fig. 2. It contains a mainboard with

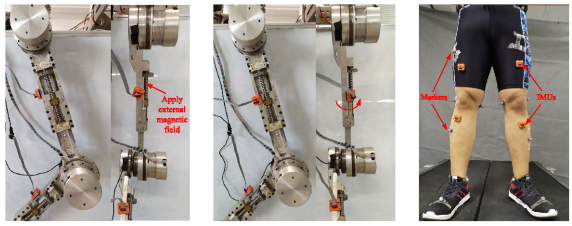

(a) Robot Test 1 (b) Robot Test 2 (c) Human Track

Fig. 3. Experiment setup for comparison in 2-DoF robot and human.

Algorithm 3: Estimation of $\hat{\phi}_1(k)$ and $\hat{\theta}_1(k)$.

Input

Latest alignment quaternion: $\hat{\mathbf{q}}_{\mathbf{b}_1}^{\mathbf{r}_1}(k)$

Angular rates from IMUs: $\mathbf{y}_w^{\mathbf{b}_1}(k)$

Acceleration from IMUs: $\mathbf{y}_g^{\mathbf{b}_1}(k)$

Last estimations: $\hat{\phi}_1(k-1)$, $\hat{\theta}_1(k-1)$

Alignment quaternion convergence flag: β_f

Output

hip joint angle: $\hat{\phi}_1(k)$, $\hat{\theta}_1(k)$

1: Calculate $\hat{\mathbf{y}}_w^{\mathbf{r}_1}(k)$ and ${}^{\mathbf{r}_1}\hat{\mathbf{w}}_{\mathbf{r}}^{\mathbf{r}_1}(k)$

2: Calculate $\frac{\mathrm{d}f_1}{\mathrm{d}\hat{\phi}_1}$ and $\frac{\mathrm{d}f_1}{\mathrm{d}\hat{\theta}_1}$ by (34), (35)

3: **if** $\beta_f == 1$ Alignment quaternions converge **then**

4: $\beta_1 = \beta_1(low)$

5: **else**

6: $\beta_1 = \beta_1(high)$

7: **end if**

8: $\Delta\hat{\phi}_1(k) = \mathbf{c}_{\mathbf{z}}^T \cdot {}^{\mathbf{r}_1}\hat{\mathbf{w}}_{\mathbf{r}}^{\mathbf{r}_1}(k)\Delta t - \beta_1 \frac{\mathrm{d}f_1}{\mathrm{d}\hat{\phi}_1}$

$\Delta\hat{\theta}_1(k) = \mathbf{c}_{\mathbf{y}}^T \cdot {}^{\mathbf{r}_1}\hat{\mathbf{w}}_{\mathbf{r}}^{\mathbf{r}_1}(k)\Delta t - \beta_1 \frac{\mathrm{d}f_1}{\mathrm{d}\hat{\theta}_1}$

9: $\hat{\phi}_1(k) = \hat{\phi}_1(k-1) + \Delta\hat{\phi}_1(k)$

$\hat{\theta}_1(k) = \hat{\theta}_1(k-1) + \Delta\hat{\theta}_1(k)$

10: $\hat{\mathbf{q}}_{\mathbf{r}}^{\mathbf{r}_1}(k) = \mathbf{q}(y, \hat{\theta}_1(k)) \otimes \mathbf{q}(z, \hat{\phi}_1(k))$

STM32F405 and two-channel CAN bus (one channel for IMUs at the left leg and the another for the right leg), a 24 V DC battery as power supply and 4 Mti-670 IMUs (Xsens Technologies B.V., The Netherlands). The IMU raw data were sampled at 100 Hz, while the three one-step gradient descent estimation algorithms were run in sequence at each sampling period to update the alignment quaternion and joint angles. The computation time for each update was tested to be about 1-2 ms.

B. Comparison in 2-DoF Robot Measurement

In order to show the performance of the proposed algorithm, we installed two IMUs in a 2-DoF robot shown in Fig. 3. The robot was controlled to move in a normal gait, with the upper joint simulating a hip and the lower joint simulating a knee. The actual joint rotational angles were measured by two encoders in the robot. Meanwhile, the joint motion were estimated by orientation outputs of IMUs and the proposed algorithm in Section III. Two experiments were conducted to verify the drift-free and self-aligned performance.

1) Magnetic Disturbance and Drift Rejection: Firstly, the IMUs were installed in the front of robot links as shown in Fig. 3(a). When the robot joints were rotating, an external magnetic field was manually applied to the IMUs. The measured and estimated angles for hip and knee joints, as well as the errors compared to the encoder measurements, are shown in the left figures of Fig. 6, 7 and 8.

It is obvious that the estimations from the proposed algorithm can steadily track the actual values in both joints, while the results from commercial IMUs with implement algorithm drifted with magnetic disturbance. Moreover, the estimation errors from the former were significantly smaller than those from the later, helped by the alignment calibration. For the method to estimate joint angles by orientations of links, the IMU body frames were not aligned to the robot joints, resulting in leak of rotational angles. However, the proposed algorithm reduced the leak with adaptive alignment.

2) Adaptive Alignment: To show the performance of adaptive alignment, the IMU attached at thigh was rotated around the link with a specific angle shown in Fig. 3(b). The middle figures of Fig. 6, 7 and 8 show the angles and estimation errors. With more serious inconsistency between IMU body and joint frames, larger leak of motion estimation by IMU implementation algorithm was generated, but the results from proposed algorithm were still unaffected.

In Fig. 4, the estimated alignment quaternions are shown to be adjusted as the knee started to rotate, which were almost optimized at the first walking step and converged at second step. With alignment, the estimated joint angular rates were identical to rotational axis, while the measured angular rates were decomposed into three axes, as shown in Fig. 5.

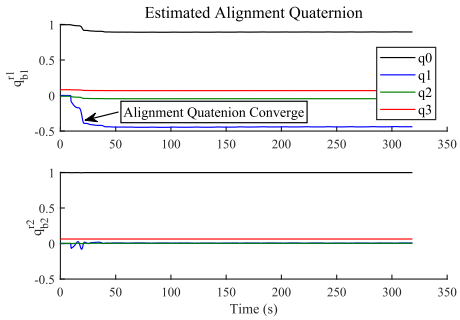

Fig. 4. Estimated alignment quaternions for hip and knee.

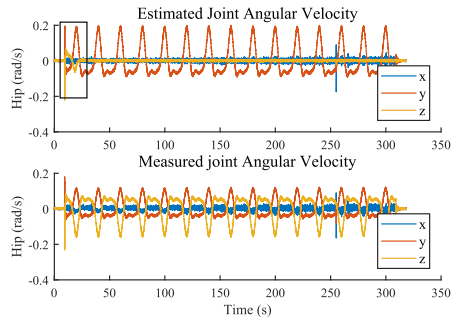

Fig. 5. Estimated and measured angular velocity for hip.

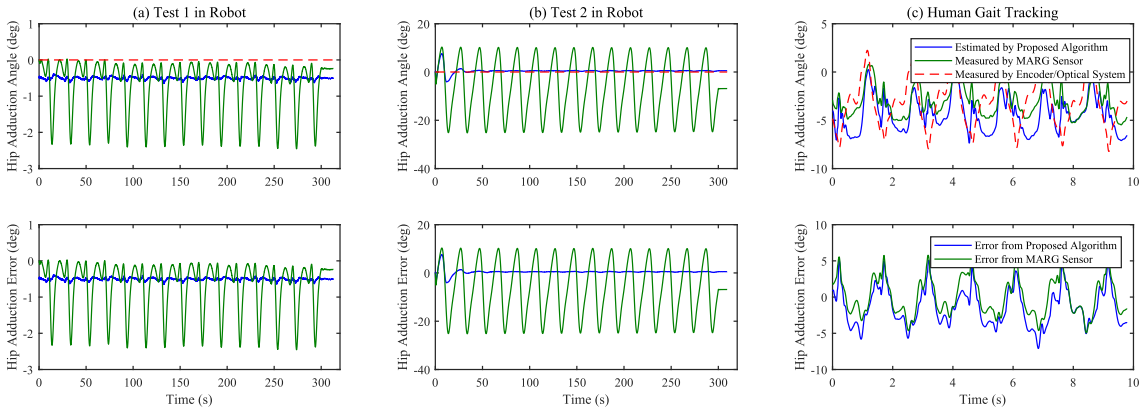

Fig. 6. Measured and estimated adduction angles for hip.

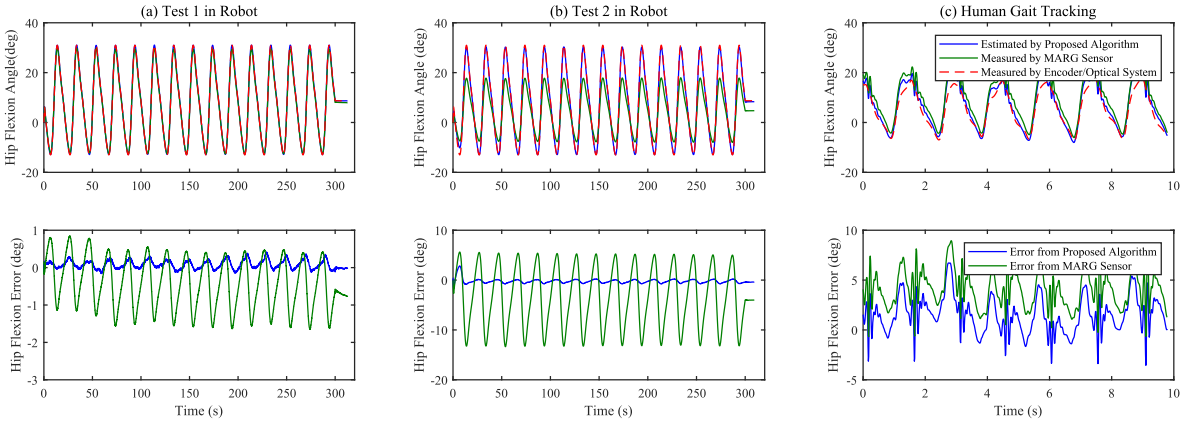

Fig. 7. Measured and estimated flexion angles for hip.

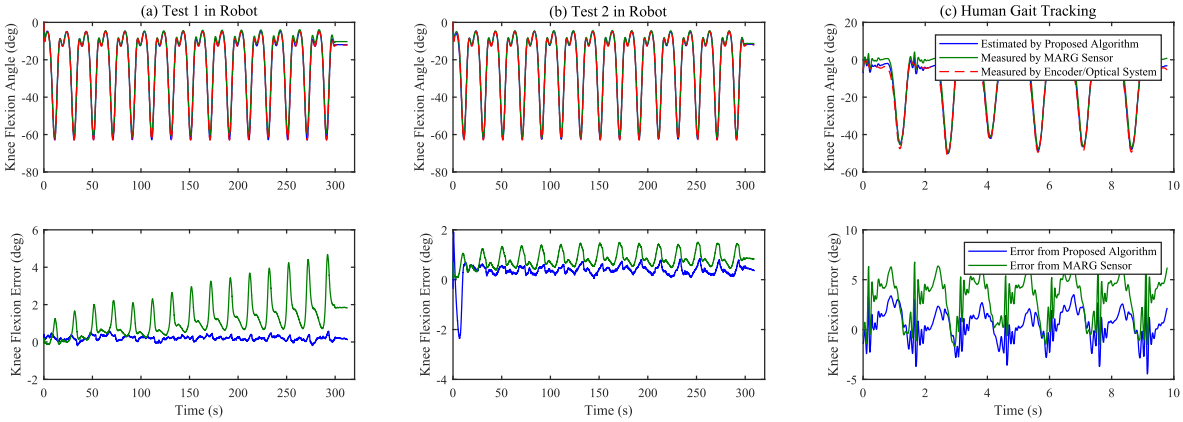

Fig. 8. Measured and estimated flexion angles for knee.The upper row shows joint angles in degree, while the lower row presents the estimation errors.

C. Comparison in Human Tracking

The IMUs were attached at a human subject to measure the joint angles, shown in Fig. 3(c), while an optical tracking system - Cortex (Motion Analysis Corporation, USA) and the biomechanics analysis tool - Visual 3D (C-Motion, Inc., USA) were used to obtain the reference gait. During the test, the human subject was walking at a treadmill in 0.45 m/s.

Shown in the right figures of Fig. 6, 7 and 8, it can be found that the estimations of knee flexion were best matched, while the hip angles produced larger estimation errors. A possible cause is the different definition of rotational sequence for hip joint and initial neutral body posture during calibration for optical tracking. In this test, the overall results were worse than those in 2-DoF robot tests, with higher fluctuation and errors. One explanation is that the joint angles from optical capture were smoothed by the process software, while the results from IMUs were not.

TABLE I
ROOT-MEAN-SQUARE ERRORS OF ESTIMATION

	Proposed Algorithm Vs Encoder/Optic			Commercial IMU Vs Encoder/Optic		
	Test 1	Test 2	Gait	Test 1	Test 2	Gait
Hip Addu	0.508°	1.126°	2.948°	0.978°	13.062°	2.621°
Hip Flex	0.142°	0.506°	2.341°	0.795°	6.934°	4.432°
knee Flex	0.237°	0.500°	1.577°	1.534°	0.878°	3.802°

Besides, there were serious noises in the original angular rate data caused by muscle movement and non-negligible disturbances to the accelerations due to the ground impact during heel strike.

D. Estimation Errors

The Root-Mean-Square estimation errors for the proposed algorithm and the commercial outputs are presented in Table I, which takes the measurements from joint encoders and the optical tracking system as reference. The results from Test 1 show that the proposed algorithm was able to obtain the joint angles with only angular velocity and acceleration data from IMUs, which was not affected by drift and magnetic disturbance. The estimate errors in Test 2 for hip joint were much smaller than those from commercial IMUs, which was beneficial from the on-line alignment. Although the results for human gait tracking were not as good as those in robot tests, it is still obvious that the proposed algorithm can estimate the human gait with acceptable accuracy.

V. CONCLUSION

In this letter, an IMU-based tracking system was designed to capture human gait. Considering the existing problems, a on-line joint angle estimation algorithm with adaptive alignment and drift rejection was proposed using only the angular rate and acceleration data. It was validated in comparison with commercial IMU outputs and measurements from joint encoders and optical tracking system, showing that the estimation accuracy is greatly improved and the method is more robust to the magnetic disturbance and misalignment.

Currently, this algorithm does not consider the probabilistic models of sensors, the performance of which much depends on the parameters in gradient descent. The segment of angular rates rather than the latest one sample could be added to improve the alignment quaternions, while Kalman filter could be designed for joint angle estimation considering probabilistic models. However, these will increase the computational costs. Apart from the alignment and drift problems that have been solved by this paper, there are other challenges in the IMU-based tracking system such as the effects of muscle movement and ground impact, resulting in severe vibrations noises and IMU movements. Therefore, better mount to attach IMUs should be designed and IMUs with lower vibration sensitivity could be considered, while filters need to be involved to process the raw measurements or estimation fluctuations by detecting heel strike states.

REFERENCES

[1] H. Zhou and H. Hu, "Human motion tracking for rehabilitation-a survey," *Biomed. Signal Process. Control*, vol. 3, no. 1, pp. 1–18, 2008.

[2] E. Chehab, T. Andriacchi, and J. Favre, "Speed, age, sex, and body mass index provide a rigorous basis for comparing the kinematic and kinetic profiles of the lower extremity during walking," *J. Biomechanics*, vol. 58, pp. 11–20, 2017.

[3] S. K. Kim, S. Hong, and D. Kim, "A walking motion imitation framework of a humanoid robot by human walking recognition from IMU motion data," in *Proc. 9th IEEE-RAS Int. Conf. Humanoid Robots*, 2009, pp. 343–348.

[4] L. Zhang, J. Sturm, D. Cremers, and D. Lee, "Real-time human motion tracking using multiple depth cameras," in *Proc. IEEE/RSJ Int. Conf. Intell. Robots Syst.*, 2012, pp. 2389–2395.

[5] G. Nagymt and R. M. Kiss, "Affordable gait analysis using augmented reality markers," *PloS One*, vol. 14, no. 2, pp. 1–15, 2019.

[6] D. Roetenberg, H. Luinge, and P. Slycke, "Xsens MVN: Full 6DOF human motion tracking using miniature inertial sensors," Xsens Motion Technologies BV, Tech. Rep, vol. 1, 2009.

[7] L. Sy *et al.*, "Estimating lower limb kinematics using a reduced wearable sensor count," 2020, *arXiv:1910.00910v3*.

[8] M. Kok, J. D. Hol, and T. B. Schn, "Using inertial sensors for position and orientation estimation," *Found. Trends Signal Process.*, vol. 11, no. 1/2, pp. 1–153, 2017.

[9] N. Trawny and S. I. Roumeliotis, "Indirect Kalman filter for 3D attitude estimation," Uni. of Min., Dept. of Comp. Sci. & Eng., Minneapolis, MN, USA, Tech. Rep. 2005-002, Rev. 57, vol. 2, 2005.

[10] J. Sola, "Quaternion kinematics for the error-state Kalman filter," 2017, *arXiv:1711.02508v1*.

[11] S. O. Madgwick, A. J. Harrison, and R. Vaidyanathan, "Estimation of IMU and MARG orientation using a gradient descent algorithm," in *Proc. IEEE Int. Conf. Rehabil. Robot.*, 2011, pp. 1–7.

[12] M. Al-Amri, K. Nicholas, K. Button, V. Sparkes, L. Sheeran, and J. L. Davies, "Inertial measurement units for clinical movement analysis: Reliability and concurrent validity," *Sensors*, vol. 18, no. 3, p. 719, 2018.

[13] G. Ligorio and A. Sabatini, "Dealing with magnetic disturbances in human motion capture: A survey of techniques," *Micromachines*, vol. 7, no. 3, 2016, Art. no. 43.

[14] X. Robert-Lachaine, H. Mecheri, C. Larue, and A. Plamondon, "Effect of local magnetic field disturbances on inertial measurement units accuracy," *Appl. Ergon.*, vol. 63, pp. 123–132, 2017.

[15] F. M. Mirzaei and S. I. Roumeliotis, "A Kalman filter-based algorithm for IMU-camera calibration: Observability analysis and performance evaluation," *IEEE Trans. Robot.*, vol. 24, no. 5, pp. 1143–1156, Oct. 2008.

[16] T. Qin, P. Li, and S. Shen, "Vins-mono: A robust and versatile monocular visual-inertial state estimator," *IEEE Trans. Robot.*, vol. 34, no. 4, pp. 1004–1020, Aug. 2018.

[17] J. Ziegler, H. Kretzschmar, C. Stachniss, G. Grisetti, and W. Burgard, "Accurate human motion capture in large areas by combining IMU-and laser-based people tracking," in *Proc. IEEE/RSJ Int. Conf. Intell. Robots Syst.*, 2011, pp. 86–91.

[18] J. A. Corrales, F. Candelas, and F. Torres, "Hybrid tracking of human operators using IMU/UWB data fusion by a kalman filter," in *Proc. 3rd ACM/IEEE Int. Conf. Human-Robot Interaction*, 2008, pp. 193–200.

[19] L. Vargas-Valencia, A. Elias, E. Rocon, T. Bastos-Filho, and A. Frizera, "An IMU-to-body alignment method applied to human gait analysis," *Sensors*, vol. 16, no. 12, 2016, Art. no. 2090.

[20] T. Seel, T. Schauer, and J. Raisch, "Joint axis and position estimation from inertial measurement data by exploiting kinematic constraints," in *Proc. IEEE Int. Conf. Control Appl.*, 2012, pp. 45–49.

[21] P. Mller, M. A. Bgin, T. Schauer, and T. Seel, "Alignment-free, self-calibrating elbow angles measurement using inertial sensors," *IEEE J. Biomed. Health Informat.*, vol. 21, no. 2, pp. 312–319, Mar. 2017.

[22] T. Seel, J. Raisch, and T. Schauer, "IMU-based joint angle measurement for gait analysis," *Sensors*, vol. 14, no. 4, pp. 6891–6909, 2014.

[23] C. Yi *et al.*, "Sensor-movement-robust angle estimation for 3-DoF lower limb joints without calibration," 2019, *arXiv:1910.07240v1*.

[24] F. Olsson, T. Seel, D. Lehmann, and K. Halvorsen, "Joint axis estimation for fast and slow movements using weighted gyroscope and acceleration constraints," 2019, *arXiv:1903.07353v1*.